NUMERICAL SIMULATION OF SOUND WAVE INTERACTION WITH HUMAN HEARING SYSTEM WITH FAST ACOUSTO-ELASTIC INTEGRAL EQUATION SOLVER

E. Bleszynski (1), M Bleszynski (1) and T. Jaroszewicz (1)

(1) Monopole Research, Thousands Oaks, Ca 913690, USA

PACS: 43.30 Ft, 43.50 Hg

ABSTRACT

We describe selected aspects of the development and applications of an elasto-acoustic fast integral solver designed to analyze sound propagation inside a human head, to examine mechanisms of energy transfer to the inner ear through air and a bone-conduction path-ways, and to assess effectiveness of noise-protection devices.

The approach uses an integral-equation formulation of acousto-elasticity and overcomes memory and execution time restrictions of conventional methods through the use of a non-lossy Fast Fourier Transform-based matrix compression algorithm parallelized on distributed-memory systems. Such a computational technique dramatically reduces both the storage and the solution time requirements: from $O(N^3)$ for the direct solution of a system of matrix equations to approximately $O(NlogN)$, where N is the number of unknowns. Effectively, the method allows one to solve the resulting discrete dense linear system representation of the integral equation with computational complexity comparable to that required to solve a sparse system of linear equations.

The developed acousto-elastic volumetric integral equation solver is capable of accurate large-scale numerical simulations involving anatomically realistic models of a human head, discretized with several million of tetrahedral elements and characterized by complex geometrical details and large density contrasts. In order to gain confidence in the solver adequacy to handle problems involving highly intricate structures of the middle and inner ear (which are essential for reliable numerical simulations capable of discerning between different mechanisms of energy transfer to the cochlea), we carried out several solver self-consistency tests (involving two different forms of integral equations) and compared its predictions with those following from an analytical solution of field distribution in an elasto-acoustic layered sphere.

We present results of representative numerical simulations of acoustic energy transfer processes to the cochlea for a human head model containing a detailed geometry representation of the outer, middle, and inner ear. The geometry model used consists of: (1) the outer surface of the skin surrounding the skull and containing (2) the outer ear represented by its exterior surface, the surface of the auditory canal, and the tympanic membrane modeled as a finite-thickness surface; (3) the middle ear, consisting of the system of ossicles and supporting structures; (4) the skull, described by external surfaces of the bones constituting the skull and including (5) a set of surfaces representing the inner ear (boundaries of the cochlea, the vestibule, and the semi-circular canals).

In addition, as an example of the code applicability to the verification of the effectiveness of noise-protection devices, we present results of numerical simulations for a model of a head protected by a helmet equipped with various material layers filling the space between the helmet and the surface of the head.

INTRODUCTION

The main objective of our development of an acousto-elastic integral equation solver is to provide a reliable numerical simulation tool for the analysis of acoustic and elastic wave propagation in the human head. Such numerical simulations can be useful, in particular, (i) in the analysis of relative importance of alternative pathways of energy transfer to the human ear, including bone and soft-tissue sound conduction, and the assessment of their role in the noise-induced damage to the human hearing system [1], (ii) in investigations of possible thermoacoustic (e.g., microwave-pulse-induced) auditory effects [2], and, (iii) in the analysis of effectiveness of noise-protection measures and noise-protective devices.

Our approach is based on an integral-equation formulation which we find, for the considered class of problems, preferable to finite-element methods both because of its accuracy and its ability of treating, without approximations, the open space (air) surrounding the object of interest.

Since an adequate discretization of geometry details of anatomically realistic models leads, immediately, to problems involving millions of geometrical elements (e.g. tetrahedroms), it poses a challenge to efficient and accurate solutions of the underlying acousto-elastic wave equations. The challenge was particularly severe for conventional integral-equation formulations whose discrete numerical representations were in terms of dense stiffness matrices.

Recently, this difficulty of conventional methods has been overcome due to the development non-lossy, error controlled matrix compression techniques, the FFT-based Adaptive Integral Method (AIM) [3] and the Fast Multipole Method (FMM) [4]. Such techniques dramatically reduce both the computational storage and the solution time requirements: from $O(N^3)$ for the direct solution of the matrix equations to approximately $O(N \log N)$, where N is the number of unknowns. Effectively, they allow one to solve a dense linear system of equations with computational complexity comparable to that required to solve a sparse one.

In the approach we describe here, we utilize the FFT-based AIM compression technique [3] initially developed in the context of elecromagnetics and adapted to acoustics [5]. This compression technique, being optimal for volumetric problems as well as problems involving sub-wavelength discretizations (tetrahedron size much smaller than the wavelength), is particularly well suited to problems involving modeling of sound wave interaction with biological tissues. In the following Sections we briefly describe the FFT-based AIM solution method and its implementation in our code, including, (i) an efficient parallelization on distributed-memory systems and, (ii) a modified integral-equation formulation which addresses nontrivial aspects of the solution technique associated with the large contrast of densities of biological tissues and the surrounding air.

We follow that discussion with a description of our approach to geometrical modeling of the human head and its auditory organs, in the context of relevant simulation tasks.

Finally, we provide examples of numerical simulations involving a human head and a helmet geometry. Results of such simulations may provide an insight into physics of sound wave propagation in nontrivial geometries of a realistically shaped human head and a helmet, and demonstrate the present capabilities of our solver.

THE NUMERICAL SIMULATION APPROACH

INTEGRAL EQUATION FORMULATION

It is a well established fact that integral-equation formulations provide the most accurate solutions to wave problems. They require, however, solving dense systems of linear equations. Traditional methods of solving such systems are characterized by computational complexity and memory requirements of the order of N^3, where N is the number of unknowns needed to adequately reproduce both the geometrical details of anatomical models and the variations of the fields. Hence, despite their reliability and accuracy, the traditional integral-equation based methods become computationally prohibitively intensive to provide solutions for realistic problems of interest.

Recently, however, a significant progress has been made in the development of fast frequency- and time-domain integral-equation solvers and, as the result, the ability of accurate and fast numerical simulations of wave propagation and scattering in complex media has dramatically improved. Suitable matrix compression techniques, the FFT-based Adaptive Integral Method (AIM) [3] and the Fast Multipole Method (FMM) [4], have been developed, which allow solving large linear sets of equations with dense matrices utilizing storage and execution times characteristic of problems involving sparse linear systems. The physical idea behind the compression methods is that interactions at large distances require less resolution than interactions at small distances. As the result, the computational complexity and memory requirements of the compression methods scale approximately linearly with the number of unknowns N.

In what follows, we describe the main features of our numerical simulation approach.

INTEGRAL EQUATION FORMULATION

SUMMARY OF THE INTEGRAL EQUATIONS IN ELASTICITY

We briefly the describe here the considered types of the integral equations we use in our simulations, and then list the general forms of the equations themselves.

(A) Volumetric integral equations. Volumetric integral equations, on the other hand, can be used for inhomogeneous media, with (generally) different material properties assigned to the individual tetrahedra into which the volume has been discretized. We use here Lippmann-Schwinger equations with the Green function associated with the infinite (unbounded) background medium – in our case, air. We consider two types of volumetric integral equations:

(i) Equations derived from differential equations in their first-order form. In this case the unknowns in the integral equations are the displacement and stress tensor fields defined in the considered volume.
(ii) Equations derived from differential equations in their second-order form. In this formulation the unknowns are only the components of the displacement field.

subparagraph(A) Equations in the "first-order" form. In the following we describe the "first-order" version of volumetric integral equations. In such a formulation, derived from the Lamé equation in its first-order form, the unknowns are the velocity $v_i := -\mathrm{i}k u_i$ (where k is the wave number in the background medium), the pressure $p := -\frac{1}{3}\tau_{kk}$, and the symmetric traceless part σ_{ij} of the stress tensor τ_{ij}. The equations involve the Green function $g(r) = \exp(\mathrm{i}kr)/(4\pi r)$ of the Helmholtz equation in the background medium, as well as its derivatives,

$$g_{mn}(\mathbf{r}) := \left(\tfrac{1}{3}\,\delta_{mn}k^2 + \partial_m\partial_n\right) g(\mathbf{r})\ . \tag{1}$$

The obtained system of integral equations, Eqs. (**??**), is then

$$\begin{aligned}
&\frac{\rho(\mathbf{r})}{\rho_0}\,v_i(\mathbf{r}) + \int \mathrm{d}^3r'\left(\partial_i\partial_m g(\mathbf{r}-\mathbf{r}')\right)\left(\frac{\rho(\mathbf{r}')}{\rho_0}-1\right)v_m(\mathbf{r}') \\
&\qquad + \frac{1}{k^2}\,\partial_m\left[\frac{\mu(\mathbf{r})}{\lambda_0}\left(\partial_i v_m(\mathbf{r}) + \partial_m v_i(\mathbf{r})\right)\right] \\
&\qquad + \frac{1}{k^2}\int \mathrm{d}^3r'\left(\partial_i g_{mn}(\mathbf{r}-\mathbf{r}')\right)\frac{2\mu(\mathbf{r}')}{\lambda_0}\,\partial'_m v_n(\mathbf{r}') + \\
&\qquad + \frac{\mathrm{i}k}{\lambda_0}\int \mathrm{d}^3r'\left(\partial_i g(\mathbf{r}-\mathbf{r}')\right)\left(\varphi(\mathbf{r}')-1\right)p(\mathbf{r}') = v_i^{\mathrm{in}}(\mathbf{r})\ , \\
&p(\mathbf{r}) - k^2\int \mathrm{d}^3r'\,g(\mathbf{r}-\mathbf{r}')\left(\varphi(\mathbf{r}')-1\right)p(\mathbf{r}') + \frac{2\mathrm{i}}{3k}\,\frac{\mu(\mathbf{r})}{\lambda_0}\,\partial_m v_m(\mathbf{r}) + \\
&\qquad + \frac{\mathrm{i}}{k}\int \mathrm{d}^3r'\,g_{mn}(\mathbf{r}-\mathbf{r}')\,\frac{2\mu(\mathbf{r}')}{\lambda_0}\,\partial'_m v_n(\mathbf{r}') = p^{\mathrm{in}}(\mathbf{r})\ , \\
&\sigma_{ij}(\mathbf{r}) - \frac{\mathrm{i}}{k}\,\frac{\mu(\mathbf{r})}{\lambda_0}\left[\partial_i v_j(\mathbf{r}) + \partial_j v_i(\mathbf{r}) - \tfrac{2}{3}\,\delta_{ij}\,\partial_m v_m(\mathbf{r})\right] = \sigma_{ij}^{\mathrm{in}}(\mathbf{r})\ ,
\end{aligned} \tag{2}$$

with a dimensionless material parameter

$$\varphi = \frac{\lambda_0}{\lambda + \frac{2}{3}\mu}\ . \tag{3}$$

We discretize the above integral equations in terms of piecewise linear basis functions. Each such basis function is associated with the vertices of the tetrahedral mesh, and supported on sets of tetrahedra adjacent to the considered vertex.

In designing our integral-equation formulation we pay a particular attention to the problem of a possible discontinuous behavior of the material properties, which is, clearly, always present when considering a mechanically dense (biological) material immersed in air.

Such problems are known to cause difficulties in solving integral equations in acoustics and, in that case, we have devised an approach [6] in which the original system of equations is reformulated in terms of a surface problem associated with the contrast interface(s) (characterized by a large ratio of densities of the adjacent materials) and a "residual" volumetric problem. The analogous problem in elasticity appears to be considerably more complex, and we have put much effort into deriving appropriate forms of integral equations, in both first- and second-order formulations ((i) and (ii) above).

Properties of the integral equations in high-contrast problems. The volumetric integral equations (2) and (**??**) have quite different (although equivalent) forms; they share, however, common features, which become relevant in problems involving large contrast. Such cases, in our applications, are characterized by large ratios of material density and the Lamé parameter λ values in the considered material and in the background medium (λ_0, with moderate values of the wave propagation speed, i.e.,

$$\frac{\rho}{\rho_0} \sim \frac{\lambda}{\lambda_0} \gg 1 \,. \tag{4}$$

In this limit only some terms in the integral equations are dominant and, moreover, they represent contributions of interfaces at which there occur large jumps in the parameters ρ and λ with respect to their background medium values ρ_0 and λ_0. This structure of the equations facilitates their discretization and solution in high-contrast problems.

(B) Surface integral equations. The surface integral equations – or boundary integral equations, BIEs – are applicable to piecewise homogeneous materials, and provide solutions for the displacement and traction fields defined on interfaces separating different material regions. Fields in the individual regions are described in terms of the appropriate Green functions for elastic materials. We use this type of equations in the following situations

1. Modeling of man-made objects of possibly complex geometrical shapes, but consisting of only few homogeneous materials.
2. Solution of the auxiliary surface problems arising in solution of the volumetric integral equations for materials characterized by large-contrast discontinuities in the material properties (we return to this problem below).
3. More generally, verification and checks of the solutions obtained with the volumetric-equations code in the case of piecewise homogeneous materials.

We first present the general form of the surface integral equations for a set of homogeneous regions Ω_m separated by interfaces; one of these regions, Ω_0, is the unbounded background medium. The displacement and traction fields are assumed to be continuous across the interfaces. The resulting system of integral equations simply consists of two equations per interface (oriented surface) S_{mn} separating the regions Ω_m (on the negative side of the interface) and Ω_n (on its positive side),

$$\begin{aligned}
&\tfrac{1}{2}\mathbf{u}(\mathbf{r}) + \int_{S_{mn}} \mathrm{d}^2 r' \left[\Gamma_m^{\mathrm{T}}(\mathbf{t},\mathbf{r}')\cdot\mathbf{u}(\mathbf{r}') + G_m^{\mathrm{T}}(\mathbf{r},\mathbf{r}')\cdot\mathbf{t}(\mathbf{r}')\right] \\
&- \sum_{\substack{S_{im}\in\partial\Omega_m \\ i\neq n}} \int_{S_{im}} \mathrm{d}^2 r' \left[\Gamma_m^{\mathrm{T}}(\mathbf{t},\mathbf{r}')\cdot\mathbf{u}(\mathbf{r}') + G_m^{\mathrm{T}}(\mathbf{r},\mathbf{r}')\cdot\mathbf{t}(\mathbf{r}')\right] = \\
&= \delta_{m0}\,\mathbf{u}^{\mathrm{in}}(\mathbf{r}) \text{ for } \mathbf{r}\in S_{mn}\,, \qquad (5a) \\
&\tfrac{1}{2}\mathbf{u}(\mathbf{r}) - \int_{S_{mn}} \mathrm{d}^2 r' \left[\Gamma_n^{\mathrm{T}}(\mathbf{t},\mathbf{r}')\cdot\mathbf{u}(\mathbf{r}') + G_n^{\mathrm{T}}(\mathbf{r},\mathbf{r}')\cdot\mathbf{t}(\mathbf{r}')\right] \\
&+ \sum_{\substack{S_{nj}\in\partial\Omega_n \\ j\neq m}} \int_{S_{nj}} \mathrm{d}^2 r' \left[\Gamma_n^{\mathrm{T}}(\mathbf{t},\mathbf{r}')\cdot\mathbf{u}(\mathbf{r}') + G_n^{\mathrm{T}}(\mathbf{r},\mathbf{r}')\cdot\mathbf{t}(\mathbf{r}')\right] = \\
&= \delta_{m0}\,\mathbf{u}^{\mathrm{in}}(\mathbf{r}) \text{ for } \mathbf{r}\in S_{mn}\,, \qquad (5b) \\
&\tfrac{1}{2}\mathbf{u}(\mathbf{r}) - \int_{S_{mn}} \mathrm{d}^2 r' \left[\Gamma_n^{\mathrm{T}}(\mathbf{t},\mathbf{r}')\cdot\mathbf{u}(\mathbf{r}') + G_n^{\mathrm{T}}(\mathbf{r},\mathbf{r}')\cdot\mathbf{t}(\mathbf{r}')bigr\right] \\
&+ \sum_{\substack{S_{nj}\in\partial\Omega_n \\ j\neq m}} \int_{S_{nj}} \mathrm{d}^2 r' \left[\Gamma_n^{\mathrm{T}}(\mathbf{t},\mathbf{r}')\cdot\mathbf{u}(\mathbf{r}') + G_n^{\mathrm{T}}(\mathbf{r},\mathbf{r}')\cdot\mathbf{t}(\mathbf{r}')\right] = \qquad (5c) \\
&= \delta_{n0}\,\mathbf{u}^{\mathrm{in}}(\mathbf{r}) \quad \text{for } \mathbf{r}\in S_{mn}\,. \qquad (5d)
\end{aligned}$$

With reference to Fig. 1, Eq.(5b) represents contributions to the displacement field $\mathbf{u}$ on the interface S_{mn} due to the displacement and traction fields $\mathbf{u}$ and $\mathbf{t}$ on the same interface (the first integral) and on other interfaces, S_{im}, forming boundaries of the region Ω_m with other regions Ω_i, $i\neq n$. These intervals involve Green functions G_m and Γ_m (defined by Eqs. (**??**) and (**??**) in Sec. **??**), describing propagation of the fields in the region Ω_m. Similarly, Eq.(5d) represents contributions to the field $\mathbf{u}$ on the interface S_{mn} due to the fields on the boundaries of the other region, Ω_n, adjacent to the interface. The r.h.s.s of Eqs. (5) are the incident fields due to distant sources in the region Ω_0 (hence the delta-functions δ_{m0} and δ_{n0}).

ELEMENTS OF THE MATRIX COMPRESSION

Our fast integral equation solver is based on the FFT-based compression method, described in detail in Ref [3, 5] The main reason for choosing the FFT-based compression method rather than the FMM approach is that it provides superior efficiency in the treatment of both volumetric problems and sub-wavelength (tetrahedron size much smaller than the wavelength) discretizations. Sub-wavelength geometry regions constitute dominant portion of the head geometry model.

The essence of the FFT-based compression is to introduce, in addition to the original basis functions (supported, e.g., on tetrahedra), an auxiliary set of far-field equivalent sources located at nodes of a regular Cartesian grid. The two coexisting representations of the basis functions, the original and the auxiliary one, are "far-field equivalent" in the sense of generating the same far-field, i.e., the field beyond the near-field-range of several tetrahedron sizes or several grid spacings (these two quantities are chosen to be of the same order). The Cartesian representation of the sources and fields leads to a Toeplitz form of the far-field component of the stiffness matrix, and allows computation of the corresponding term in the matrix-vector product by means of FFTs. At the same time, the near-field of the matrix is, by construction, sparse. Thus, the complexity of the matrix-vector product is reduced from $O(N^2)$, characteristic of a dense matrix, to $O(N\log N)$.

ELEMENTS OF THE PARALLELIZATION

An indispensable element of the solver is its parallel implementation designed for distributed-memory systems, such as PC clusters. It includes a parallel implementation of three dimensional FFTs, based on the FFTW package [7] which, in

spite of the massive all-to-all communication involved in one of its stages, achieves a near-perfect scaling on parallel, distributed memory architectures (in our computations, equipped with the InfiniBand interconnect network) up to thousands of processors.

Other elements of the solver have also been designed to fully scale with the number of processors, in both storage and computation time. This feature is mostly due to a partitioning of the object geometry, in our case, into "slices" defined in terms of one of the coordinates of the Cartesian grid. In this way, each processor handles primarily only one geometry slice and, in some auxiliary operations, at most few of the adjacent slices.

Our solver implements a volumetric integral-equations approach in which, depending on the choice of the basis functions and the specific form of the equations, the unknowns are displacements, components of the stress tensor, or pressures associated with nodes or with tetrahedra of a volumetric tetrahedral mesh.

In addition to utilizing the FFT-based matrix compression and parallelization, the solver employs a formulation different from conventional Lippmann-Schwinger integral equations, and better suited to large density contrast problems [6]. The improved solution scheme consists of (i) casting integral equations into a form which exhibits separation of volume and surface components; (ii) solving the surface problem; (iii) solving the volumetric problem with a new source term defined in terms of the obtained surface solution; and (iv) constructing the final solution as a proper combination of the surface and volume solutions. The implemented procedure is rigorous and does not suffer from ill-conditioning in the limit of large density contrasts. Its application is essential in problems involving biological tissues in air (i.e., density ratios exceeding 1000).

THE GEOMETRICAL MODEL AND MECHANICAL PROPERTIES OF MATERIALS

We constructed a simple, yet relatively realistic geometrical model of a human head consisting of skin, skull and brain tissue, with the cochlea embedded in the skull. We also constructed a model of a helmet and a padding material placed between the head and the interior of the helmet surface. The components of the model are shown in Figs. 2 and 3.

The above elements constitute a minimal yet relevant set of geometry components required in carrying out simulations of energy deposited within the cochlea region and, subsequently, in the determination of auditory effects of the propagating wave. The helmet geometry allows us to investigate the influence of the padding material, as well as of possible air gaps between the head and the helmet structure on the energy distribution inside the head model.

Our present parallelized version of the solver allows us to obtain solutions for such models, discretized with several million of unknowns, within the time span of a few hours.

EXAMPLES OF REPRESENTATIVE NUMERICAL SIMULATIONS

In this Section we present some preliminary illustrations of the capabilities of our solver.

In Fig. 4 we show pressure distribution in a human head model in the presence and the absence of a helmet. We assumed a steel helmet and the space between the helmet and the head filled with cork. Frequency of the harmonic acoustic wave, incident laterally on the right ear of the head model was 5 kHz. Geometries were discretized with tetrahedron sizes (edge lengths) of about 3 mm, resulting in (a) $N \simeq 2,700,000$ tetrahedra for the head, and (b) $N \simeq 4,700,000$ for the head and helmet system. The computations were carried out on a Linux cluster with the InfiniBand interconnect network, on 108 processors for the model (a) and 128 processors for the model (b). The total computation times were (a) about 50 minutes and (b) about 2 hours, the longer time for the case (b) due mostly to the larger number of iterations in the solution. One iteration required 4.6 s in the problem (a) and 6.6 s in the problem (b). We estimate that, in both cases, the overall computation time can be reduced by 30 to 50 % by optimizing the matrix construction stage of the code.

The results show a nontrivial behavior of the solutions and exhibit physical phenomena which may be relevant in the design of protective devices.

In the case of the head, Fig. 4(a), the pressure is maximal at the entrance to the ear canal, and it is relatively smoothly distributed inside the head. In fact, the solution is suggestive of a resonance-type (P-wave) behavior: the pressure changes sign along the approximately vertical line seen in the Figure.

The solution for head and helmet system, Fig. 4(b), is quite different. It exhibits a distinct oscillatory behavior along the surface of the helmet and in the region filled by cork. This region appears to have properties of a "waveguide'. Because of the cork density being significantly lower than that of the surrounding materials (the helmet and the head), and the resulting impedance mismatch at the boundaries, the wave tends to be trapped in that region. Since the refractive index of cork is not much different from that of air, wave oscillations are relatively rapid. We stress, however, that the physical picture suggested by Fig. 4(b) would change if we included dissipative (attenuation) effects in the filling material, e.g., if we considered a strongly damping porous material characterized by a complex refractive index.

We note that, for the particular frequency considered here, the presence of a helmet completely changes the pressure distribution in the head, but does not reduce its maximum value (we note that the data Figs. 4(a) and Fig. 4(b) are plotted in different scales).

SUMMARY

We described our approach to numerical simulation of acoustic and elastic wave propagation in the human head based on integral equation formulation and, applicable to quantitative assessment of the importance of various energy transfer mechanisms (such as bone conduction), effects of noise and noise protection measures. Our a fast, parallelized volumetric integral-equation solver allows efficient treatment of large scale problems discretized with millions of tetrahedral elements. In order to get confidence into able numerical simulations capable of discerning between different mechanisms of energy transfer to the cochlea), we carried out several solver self-consistency tests (involving two different forms of integral equations) and compared its predictions with those following from an analytical solution of field distribution in an elasto-acoustic layered sphere. We illustrated these developments with preliminary computation results showing effects of a helmet enclosing a human head model, and exhibiting a nontrivial behavior of the solution for realistic geometries.

ACKNOWLEDGMENT

This work is supported by a grant from US Air Force Office for Scientific Research

REFERENCES

[1] E. H. Berger and R. W. Kieper, "Hearing protection: Surpassing the limits to attenuation imposed by the bone-conduction pathways," *J. Acoust. Soc. Am.*, vol. 114, pp. 1955–1967, 2003.

[2] J. A. Elder and C. K. Chou, "Auditory response to pulsed radiofrequency energy," *Bioelectromagnetic Supplement*, vol. 6, pp. S162–S173, 2003.

[3] E. Bleszynski, M. Bleszynski, and T. Jaroszewicz, "AIM: Adaptive Integral Method for solving large-scale electromagnetic scattering and radiation problems," *Radio Science*, vol. 31, pp. 1225–1251, 1996.

[4] R. Coifman, V. Rokhlin, and S. Wandzura, "The Fast Multipole Method for the wave equation: a pedestrian prescription," *IEEE Antennas and Propagation Magazine*, vol. 35, pp. 7–12, 1993.

[5] E. Bleszynski, M. Bleszynski, and T. Jaroszewicz, "Fast volumetric integral solver for acoustic wave propagation through inhomogeneous media," *J. Acoust. Soc. Am.*, vol. 124, pp. 396–408, 2008.

[6] ——, "Fast volumetric integral-equation solver for high-contrast acoustics," *J. Acoust. Soc. Am.*, vol. 124, pp. 3684–3693, 2008.

[7] M. Frigo and S. G. Johnson, *FFTW manual for version 3.2alpha3*, Massachusetts Institute of Technology, August 2007.

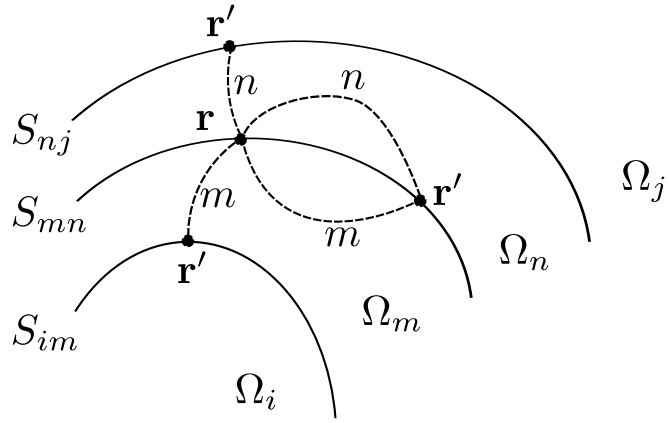

Figure 1: A schematic representation of regions Ω and interfaces S appearing in integral equations 5.

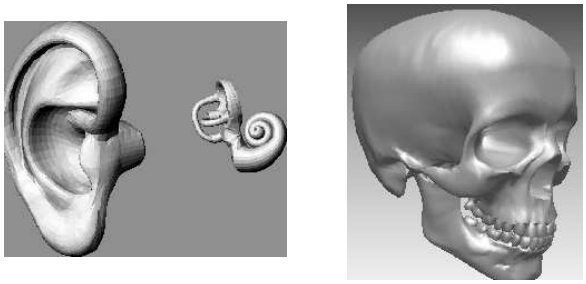

Figure 2: The external ear, the cochlea, and the skull models used in the simulations.

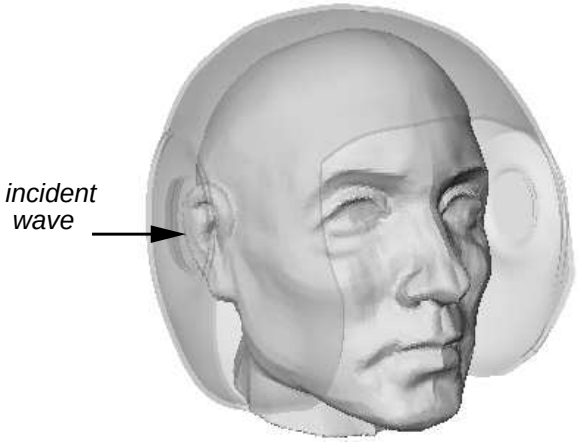

Figure 3: Model of the external head surface and the helmet. The arrow indicates the direction of the incident wave.

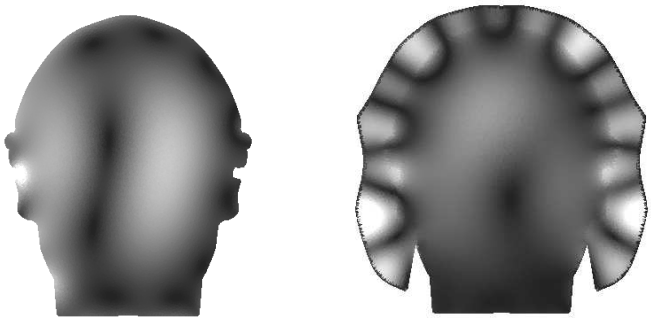

(a) (b)

Figure 4: Pressure distributions in the coronal plane for (a) the human head model and (b) the system consisting of the human head model and a steel helmet, with the in-between space filled by cork. The models are subject to an acoustic wave of unit pressure amplitude and frequency 5 kHz, incident from the left. The maximum pressure value is about 4 in (a) and 15 in (b).

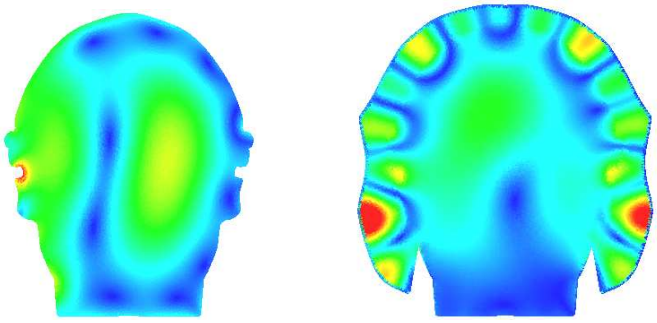

(a) (b)

Figure 5: Pressure distributions in the coronal plane for (a) the human head model and (b) the system consisting of the human head and a steel helmet models, with the in-between space filled by cork. The models are subject to an acoustic wave of unit pressure amplitude and frequency 5 kHz, incident from the left. The maximum pressure value is about 4 in (a) and 15 in (b).